Journal of Materials Research and Technology 35 (2025) 4520–4533

Contents lists available at ScienceDirect

Journal of Materials Research and Technology

journal homepage: www.elsevier.com/locate/jmrt

A dislocation-based model for the substructure evolution and flow stress of aluminum alloys during high-temperature compression

Qi Yang, Tomasz Wojcik, Ernst Kozeschnik *

Institute of Materials Science and Technology, TU Wien, Getreidemarkt 9, 1060, Vienna, Austria

ARTICLE INFO

Keywords:
Microstructure evolution
Hot deformation
Dynamic recrystallization
Dynamic recovery
Dislocation density
Physical modeling

ABSTRACT

The microstructure evolution of aluminum alloys during plastic deformation is a complex metallurgical process controlled by interacting physical mechanisms, such as recovery, continuous dynamic recrystallization (CDRX), and substructure evolution. The present study proposes a dislocation-based model framework to describe the microstructural evolution of dislocation density, subgrain size, misorientation angle, and flow stress. The wall dislocation density is modeled on the basis of the average subgrain size and misorientation evolution. The dislocation density and substructure evolution are independently simulated and compared with electron backscatter diffraction (EBSD) experimental results. Their mechanisms are thoroughly discussed. The decrease in low-angle subgrain size and the increase in the misorientation angle of subgrain boundaries with increasing strain rate, as well as their evolution with temperature and strain rate, are well reproduced over a wide range of large strains. Furthermore, the evolution of these experimental substructures is employed to model other related mechanical properties. The framework is successfully applied and validated for AA1050 and AA5052 aluminum alloys across different deformation conditions.

1. Introduction

Numerous researchers [1–8] have studied the microstructure evolution laws under various conditions for high-stacking fault energy materials, such as aluminum alloys, indicating that recovery and dynamic recrystallization (DRX) are essential softening mechanisms during hot forming. Recovery is a softening process during which defects, primarily dislocations, are either annihilated or rearranged to reduce the internal energy of the material [9–11].

Consequently, continuous deformation contributes to an increased misorientation of low-angle subgrain boundaries (the critical misorientation angle set as 15°), which progressively transform into high-angle grain boundaries (HAGBs) with misorientation angles exceeding 15°, as observed in continuous dynamic recrystallization (CDRX) [12–14]. CDRX is the most common mechanism observed in Al alloys during hot forming. The other two forms are discontinuous dynamic recrystallization (DDRX) [15,16] and geometric dynamic recrystallization (GDRX) [17,18]. In contrast to DDRX, CDRX is a non-nucleation process, the primary mechanism of CDRX being the continuous rotation of subgrains [19,20].

Understanding and modeling complex dislocation density reactions are the keys to controlling DRX and the deformation behavior of Al alloy. Several approaches [21–24] are reported in the literature describing the dislocation density evolution and the flow curves of aluminum alloys during hot deformation.

The dislocation density-based models for metal plasticity rely on the work of Kocks [25], Bergström [26], Bergström and Roberts [27], and Mecking and Estrin [28]. Kocks and Mecking [29] modeled and reviewed the dislocation-mediated flow stress with dislocation accumulation and annihilation during the deformation of FCC metals, called the Kocks and Mecking (KM) dislocation model, which is the basis of many subsequent microstructure evolution models. Roters et al. [30] established a new work-hardening model for homogeneous and heterogeneous cell-forming alloys. They distinguish three internal state variables in terms of three categories of dislocations: mobile and immobile dislocations in the cell interiors and immobile dislocations in the cell walls. Hughes and Hansen [31,32] investigated and modeled the deformation structures and the microstructural origins by classifying low angle incidental dislocation boundaries (IDBs) and medium to high angle geometrically necessary boundaries (GNDs) during work hardening stages.

Estrin et al. [33] introduced a novel dislocation model to

* Corresponding author.
E-mail address: ernst.kozeschnik@tuwien.ac.at (E. Kozeschnik).

https://doi.org/10.1016/j.jmrt.2025.02.132
Received 13 December 2024; Received in revised form 10 February 2025; Accepted 14 February 2025
Available online 15 February 2025

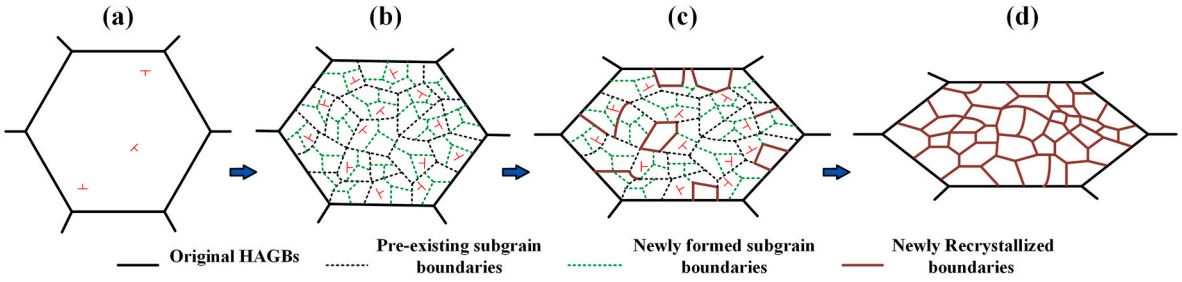

Variables \ Evolution	Step (a)	Step (b)	Step (c)	Step (d)
Excess Dislocation density ρ	0	↑	↓	Constant
δ_{sub}	None	↓	δ_{DRX}	Constant
X_{DRX}	0	0	↑	=100%
Subgrain misorientation θ	0°	>2° ↑	Some>15° ↑	Constant
D	D0	D0	↓	δ_{DRX}

Fig. 1. Illustration of the microstructure evolution during continuous compression: (a) initial microstructure before deformation; (b) generation of cells and sub-grains; (c) generation of recrystallized grains; (d) full recrystallization state.

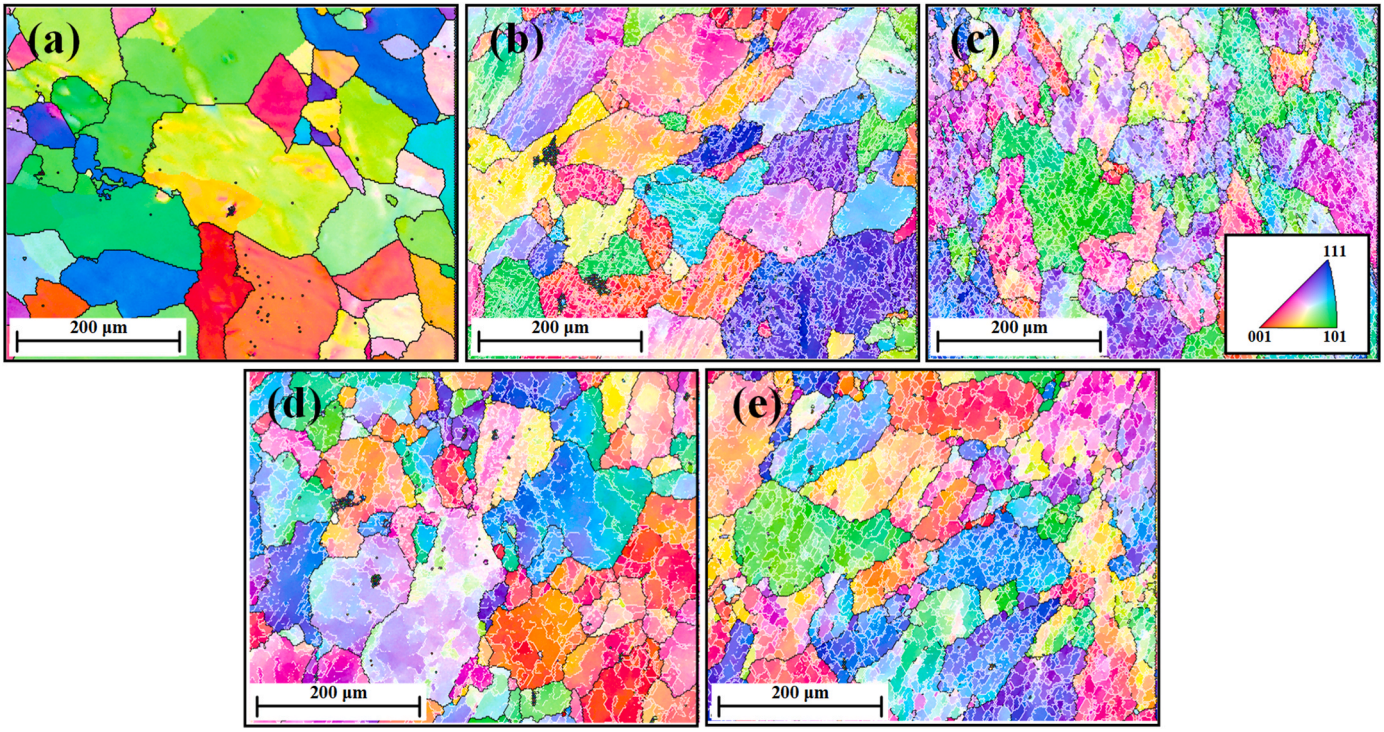

Fig. 2. Electron backscatter diffraction (EBSD) images of AA1050 Al alloy deformed to a different strain: (a) inverse pole figure (IPF) maps of the undeformed specimen, (b)–(c) IPF maps of the specimens deformed with strain 0.3 and 0.6 (at a temperature of 300 °C and a strain rate of 0.1 s^{-1}), and (d)–(e) IPF maps of the specimens deformed with strain 0.3 and 0.6 (at 400 °C/0.1 s^{-1}).

characterize the hardening behavior of cell-forming crystalline materials under large strains, which incorporates a cellular dislocation structure consisting of cell walls and cell interiors. Toth et al. [34] also developed a dislocation based polycrystal plasticity model to explain strain hardening at large strains, incorporating interiors and wall dislocation densities. Recently, Toth and Rollett [35] proposed a strain hardening model for deformation stage IV recently, which accounts for lattice curvature-induced dislocations, including variations in geometrically necessary dislocation (GND) density across different deformation stages. These dislocation models are established for large strains, which also provide valuable insights into the underlying mechanisms and comparison with elevated temperature conditions.

Material models for DDRX-based microstructure evolution are frequent in the literature [36–38], whereas physical models of substructure evolution and subsequent CDRX processes are relatively scarce. A physically-based CDRX model was proposed by Gourdet and Montheillet [39], the GM model, which considers the average dislocation density, the average crystallite size, and subgrain boundary misorientation. Sun et al. [40] modified the GM model by adding subgrain boundary area, recrystallized grain boundary area, and high-angle grain boundary area as internal-state variables. Chen et al. [41] modified the GM model with a coupled CDRX-VPSC (visco-plastic self-consistent) model that employs dislocation density. Buzolin et al. [42] developed a microstructure model for two-phase titanium alloys, comprising microstructure, yield stress, constitutive equations, plastic strain partitioning, and rate equations for the internal variables. Furthermore, Ferraz et al. [43], Liu et al. [44] and Wang et al. [45] have also developed models using mesoscale model, recently, based on the GM model. Among the proposed dislocation-based model for Al alloys, either a large number of non-physical fitting parameters are used extensively, or the actual microstructure evolution is not integrated. In this study, several innovative independent dislocation-based models are introduced incorporating micro/substructural evolution parameters directly, incorporating physically meaningful variables, is applied based on experimental values.

The present work proposes a dislocation-based model framework to reproduce dislocation population dynamics and microstructural evolution in Al alloys with elevated temperature conditions. The dislocation model accounts for work hardening and various annihilation mechanisms within cell interiors. A wall density model is established by incorporating substructure evolution calculations. The microstructural evolution laws are simulated as functions of temperature, strain, and strain rate. The models are individually analyzed and validated against independent experimental data, showing good agreement between the simulations and experiments in a large range of strain.

2. State of the art

Fig. 1 illustrates the microstructure evolution during continuous compression. The initial microstructure, before deformation, consists of a parent structure with a low number of pre-existing dislocations (Fig. 1a). As deformation commences, the accumulation and rearrangement of tangled dislocations lead to the formation of newborn cells and subgrains through DRV (Fig. 1b). These subgrains gradually increase their boundary misorientation due to subgrain rotation, ultimately converting some of the low-angle subgrains into HAGBs [39] (Fig. 1c). Additionally, as the subgrains absorb dislocations, their misorientation further increases, as suggested by Huang and Logé [10]. With continued compression, the microstructure eventually reaches a steady state.

The microstructure evolution and associated discussions have been studied in some literature [1–10] and the author's publication [20,46], which demonstrates the formation of a well-defined substructure and subsequent DRX. Fig. 2 show the microstructure maps after compression under various deformation condtions (refer to Section 4.2.1). Low-angle subgrain boundaries and high-angle grain boundaries (HAGBs) are shown as white and black lines, respectively. The main microstructural evolution mechanisms observed in Al alloys based on both existing studies and our experimental observations, can be summarized as follows:

(i) Mobile dislocations with a density ρ accommodate plastic deformation. The changes in density stem from the balance between their generation, annihilation, and transformation into wall dislocations. As shown in Fig. 2, the accumulation of dislocations into low-angle subgrain boundaries with forming a substructure by dynamic recovery (DRV) [9–11], which is often referred to as wall dislocations. Additionally, interior dislocations within the grain also annihilate during processes such as DRV, static recovery (SRV), or recrystallization. For instance, dislocation annihilation occurs when dislocations approach each other within a critical distance during DRV. Mathematical models of dislocation density often incorporate these evolutionary processes, such as KM model [29] and ABC model [23].

(ii) The formation of newborn subgrain boundaries resulting in a rapid reduction in the average subgrain size as the misorientation angle increases. Previous papers by the authors [46] have revealed that the average subgrain size depends on factors such as temperature, strain rate, and strain, in agreement with studies from Poletti [47] and Nes [48]. The average subgrain size δ_{sub} decreases with deformation and reaches a "saturation value" at large strains in literature [46,49].

(iii) The misorientation angle of subgrains θ gradually increases to a critical angle with the evolution of dislocation density and subgrain size [9–11]. Studies indicate that the acceleration of misorientation at subgrain boundaries occurs at low strain rates. Furthermore, higher temperatures can either increase or decrease the steady-state value of misorientation, depending on the temperatures and material properties [10,20]. The misorientation angle of subgrain boundaries is strongly correlated with the accumulation of dislocation density, as well as the formation and size reduction of these boundaries.

(iv) DRX can occur during the hot compression of Al alloys, consistent with the author's published research [20], with the DRX fraction X_{DRX} increasing as the misorientation of low-angle subgrains increases, leading to their progressive transformation into HAGBs.

(v) The average grain size D continues to decrease from the initial mean grain size D_0 until complete recrystallization is achieved, resulting in a newly recrystallized grain size δ_{DRX} [10,50]. A reduction in the initial grain size can significantly enhance the kinetics of grain refinement during large strain deformation [51]. Similarly, smaller initial grain sizes and low-angle subgrain size facilitate a more rapid attainment of stable subgrain size value, as evidenced by the results of the current physical model (refer to Section 4.2.4).

These variables are incorporated into the present dislocation-based CDRX model for Al alloys to simulate the microstructure evolution under various deformation conditions. The work primarily develops models for interior and wall dislocation densities, average subgrain size, subgrain boundary misorientation, and flow stress based on substructure evolution.

3. Model development

3.1. Dislocation density evolution model

In high-stacking fault energy materials, such as Al alloys, dislocations can arrange themselves into well-organized cell or subgrain structures with continued deformation, leading to the gradual increase of subgrain misorientation [9,10]. The wall dislocation density of subgrain boundaries strongly depends on the various deformation parameters.

In the present work, the proposed evolution models incorporate dislocation density, average subgrain size, and subgrain misorientation angle as internal variables representing the material's microstructure. The total dislocation density (ρ_t) is divided into two populations: the interior dislocations with a density ρ_i and the wall dislocations with a density ρ_w. The interior dislocation density represents the dislocations within parent grains and newly formed subgrains, while the wall dislocation density represents the dislocations at the newly formed cell or subgrain walls.

Considering the rule of mixtures applied to two populations, the total dislocation density (ρ_t) can be calculated as

$$\rho_t = f_i\rho_i + f_w\rho_w, \tag{1}$$

where f_i represents the material coefficient related to the fraction of interior dislocations, and f_w is a material coefficient related to the fraction of wall dislocations, with $f_i + f_w = 1$.

The interior dislocation density model incorporates several mechanisms that determine the dislocation evolution. It is described with the ABC dislocation model [23,52,53] and the GM model [39]. This model mainly describes the following evolution processes: work hardening (WH), the reduction of dislocation density through DRV and static recovery (SRV), as well as the average dislocation density reduction caused by HAGBs movement as

$$d\rho_i \Big/ dt = \frac{M\sqrt{\rho_i}}{Ab}\dot{\varepsilon} - 2BM\rho_i\frac{d_{crit}}{b}\dot{\varepsilon} - 2CD_d\frac{Gb^3}{k_BT}\left(\rho_i{}^2 - \rho_{eq}^2\right) - 2f_H v_H \rho_i \frac{1}{\delta_w}, \tag{2}$$

where A, B and C are material-dependent coefficients, M is the Taylor factor, G the shear modulus, b the Burger's vector, $\dot{\varepsilon}$ the strain rate, k_B the Boltzmann constant, T the deformation temperature, d_{crit} the critical distance of dislocation annihilation, D_d the diffusion coefficient along dislocation pipes, ρ_{eq} is the equilibrium dislocation density, δ_w the average size (diameter) of low-angle walls/subgrains, f_H the fraction of HAGBs, and v_H is the migration rate of HAGBs.

The last term in eq. (2) accounts for the reduction of the average internal dislocation density accompanying the migration of HAGBs. Following the GM model [39], the migration rate v_H of aluminum follows a power-law function of the strain rate, exhibiting minimal temperature dependence. The driving force generated by differences in local dislocation density increases with the strain rate. The rate of HAGBs is adopted from Gourdet and Montheillet [39] as

$$v_H = v_0\left(\frac{\dot{\varepsilon}}{\dot{\varepsilon_0}}\right)^m, \tag{3}$$

where $\dot{\varepsilon_0}$ is the initial value of the strain rate, v_0 the initial migration rate of HAGBs, and m is a material constant related to the migration rate.

The average dislocation annihilation due to DRV occurs when two dislocations with antiparallel Burgers vectors approach each other within a critical distance d_{crit}, leading to their annihilation. The critical distance d_{crit} can be theoretically derived from the dislocation annihilation mechanism, which is expressed as [54]

$$d_{crit} = \frac{Gb^4}{2\pi(1-\nu)Q_{vac}}, \tag{4}$$

where ν is the Poisson's ratio, and Q_{vac} is the vacancy formation energy.

The diffusion coefficient along dislocation pipes D_d can be expressed as [55]

$$D_d = D_{d0}\exp\left(\frac{Q_d}{RT}\right), \tag{5}$$

where D_{d0} is the pre-exponential factor for pipe diffusion, Q_d is the activation energy for pipe diffusion, and R is the gas constant.

Since dislocation generation continues while deformation proceeds, an increasing number of dislocations are piled up, leading to the formation of new low-angle subgrains/LAGBs [9–11]. The evolution of the wall dislocation density is directly considered with changes in the corresponding substructure variables, reproducing the expected evolution of substructure and dislocations using physically based parameters. The wall dislocation density model is represented as the total length of wall dislocation lines per unit volume, expressed as [56].

$$\rho_w = \frac{\sum_1^i L_{wi}}{\sum_1^i V_{wi}} = f_s\frac{\theta_{wi}}{2b}r_i, \tag{6}$$

where L_{wi} is the total length of wall dislocation lines of the i-th subgrain wall, V_{wi} is the total volume of the i-th subgrain wall, θ_{wi} is the average misorientation angle of the i-th subgrain wall, r_i is the ratio of subgrain surface to subgrain volume of the i-th subgrain wall, and f_s is a materials coefficient related to the subgrain boundary fraction.

Following the Peŝiĉka et al.'s model [56], only subgrain boundaries with misorientation angles of less than 5° are considered. According to current literature [9–11], the critical misorientation angles for small-angle and high-angle subgrain boundaries after recrystallization are set as 15°, leading to higher dislocation densities at these boundaries (cell walls). Additionally, the model assumes that micro-grains exhibit elongated shapes, with an average aspect ratio of 4:1 (length to width), which also introduces higher dislocation densities along the elongated direction in the model calculations compared to the hypothetical subgrains proposed in this study. Consequently, the value of f_s is set to 1/8 in the present work.

Subsequently, we assume that low-angle subgrains exhibit hypothetical shapes with a diameter of δ_w, which can be determined from EBSD data. Detailed measurements of subgrain sizes are available in previous publications [46]. A mean-field model concept is then introduced by calculating the surface area and volume of spherical subgrains. The average low-angle subgrain size (diameter of subgrains), denoted as δ_w and the subgrain misorientation angle θ_w are introduced for modeling, allowing the wall dislocation density to be expressed as

$$\rho_w = f_s\frac{\theta_w}{2b}\pi\delta_w{}^2 \Big/ \left(\frac{4}{3}\pi\left(\frac{\delta_w}{2}\right)^3\right), \tag{7}$$

where θ_w is the average misorientation angle of subgrain (cell) walls.

3.2. Subgrain size evolution model

The high-temperature deformation of Al alloys typically occurs in three stages [1,9,10,48]: (i) An initial stage where cells/subgrain boundaries are formed, followed by (ii) subgrain refinement and (iii) thermal coarsening of subgrains. The substructure-based model for the

Table 1
List of input parameters for AA1050 Al alloy.

Symbol	Name	Unit	Value	Ref.
ν	Poisson's ratio	–	0.347	[65]
G	Shear modulus	MPa	29438.4−15.052T	[66,67]
b	Burgers vector	m	$2.86{\cdot}10^{-10}$	[68]
M	Taylor factor	–	3.06	[69]
Q_{vac}	Activation energy for vacancy formation	eV	0.67	[70]
Q_d	Activation energy for pipe diffusion	J.mol^{-1}	$83.2{\cdot}10^{3}$	[55]
D_{d0}	Pre-exponential factor for pipe diffusion	m^2.s^{-1}	$1.5{\cdot}10^{-6}$	[55]
ν_D	Debye frequency	s^{-1}	$1{\cdot}10^{13}$	[48]
A	A parameter	–	$1.8{\cdot}\exp(0.0066T)$	This work
B	B parameter	–	3	This work
C	C parameter	–	$1{\cdot}10^{-3}$	This work
f_r	Material coefficient related to subgrain refinement	–	$3.5{\cdot}10^{9}[\dot{\varepsilon}{\cdot}\exp(Q/RT)]^{-0.21}$	This work
f_c	Material coefficient related to subgrain coarsening	–	$10000[\dot{\varepsilon}{\cdot}\exp(Q/RT)]^{0.55}$	This work
f_i	Fraction of interior dislocations	–	0.95	This work
f_w	Fraction of wall dislocations	–	0.05	This work

average subgrain size evolution has been reported in a previous paper and literature [46,48,57] and reads

$$d\delta_w \Big/ dt = -f_r\frac{\sqrt{3}\dot{\varepsilon}b^{1/2}}{\overline{\theta}_s^{\,3/2}\overline{\delta}_s^{\,2}}\delta_w^{\nu_1} + f_c\nu_D b^2\sqrt{\rho_t}\left[\exp-\left(\frac{U_s - PV_a}{k_B T}\right)\right], \tag{8}$$

where ν_D is the Debye frequency, P the driving force on the subgrain boundary, V_a the average activation volume for subgrain boundary movement, U_s the activation energy for self-diffusion in Al, f_r and f_c are material coefficients related to the subgrain evolution, $\overline{\theta}_s$ is the average subgrain boundary misorientation in the steady-state stage, ν_1 a material coefficient that controls the subgrain refinement rate and which is set to 1 in the present work, and $\overline{\delta}_s$ is the average subgrain size in the steady-state stage.

The driving force for subgrain coarsening is governed by the evolution of subgrain boundary energy and subgrain size, as described in Eq. (9). In this equation, the prediction of subgrain boundary energy is performed using the Read-Shockley relationship [48,57,58] with

$$P = \frac{4\gamma}{\delta_w}, \text{with } \gamma = \gamma_m\frac{\theta_w}{\theta_m}\left(1 - \ln\left(\frac{\theta_w}{\theta_m}\right)\right), \tag{9}$$

where γ represents the subgrain boundary energy, γ_m is the boundary energy of HAGBs, and θ_m is the misorientation angle at which a boundary is defined as a HAGB, typically taken as 15°.

The activation volume for subgrain boundary movement is determined by the average misorientation angle, which is used as [48].

$$V_a = \frac{b^3}{\theta_w} \tag{10}$$

3.3. Misorientation angle evolution model

In section 3.1, we evaluate the dislocation density evolution during DRV and SRV. Following the methodology of Gourdet and Montheillet [39], the calculation incorporates both the annihilation and transformation of dislocations during recovery. A fraction α_s of the dislocations is removed by recovery, while the remaining fraction $1-\alpha_s$, contributes to the formation of new subgrains and an increase of the misorientation angle. The rate of the dislocation density during deformation and subgrain rotation is then [39]

$$d\rho_{sr} \Big/ dt = \frac{(1-\alpha_s)}{\alpha_s}\left(2BM\rho_i\frac{d_{crit}}{b}\dot{\varepsilon} - 2CD_d\frac{Gb^3}{k_B T}\left(\rho_i{}^2 - \rho_{eq}^2\right)\right), \tag{11}$$

where ρ_{sr} represents the total recovered dislocation density involved in subgrain rotation, and $1-\alpha_s$ is the fraction of recovered dislocations that participate in subgrain rotation. This quantity is taken as 0.5.

Subsequently, an extended subgrain misorientation angle model is developed that considers various factors, including the dislocation density, strain rate, average subgrain size, and subgrain boundary energy. The equation reads as

$$d\theta_w \Big/ dt = f_\theta\frac{b\dot{\varepsilon}\delta_w}{2n}\frac{(1-\alpha_s)}{\alpha_s}\left(2BM\rho_i\frac{d_{crit}}{b}\dot{\varepsilon} - 2CD_d\frac{Gb^3}{k_B T}\left(\rho_i{}^2 - \rho_{eq}^2\right)\right)\gamma^{c_2}, \tag{12}$$

where n is the number of dislocation pairs within the boundary, with a value of 3 as suggested by Gourdet and Montheillet [39]. c_2 is a material constant that describes the relationship between the average misorientation angle and the subgrain boundary energy, and f_θ is a material coefficient related to the saturated misorientation angle.

Numerous researchers have observed that the average misorientation of subgrains consistently reaches a steady-state value of about 4°–8° for aluminum alloys when subjected to critical strain levels [10,59,60], such that the misorientation angle is no longer sensitive to increasing deformation strain, since $d\theta_w/dt = 0$. Consequently, a material coefficient f_θ is introduced into the model, with the saturated misorientation angle θ_{sat} being expressed as

$$f_\theta = c_3\left(1 - \frac{\theta_w}{\theta_{sat}}\right), \tag{13}$$

where c_3 is a material constant that describes the relationship between the average misorientation angle and the saturated misorientation angle. θ_{sat} is the saturated misorientation angle with continuing deformation.

3.4. Constitutive model

Here, various strengthening theories are employed to describe the relationship between macroscopic flow stress and the microstructure of an AA1050 Al alloy, focusing on the basic yield strength and dislocation strengthening mechanisms. The contributions of two types of dislocations (interior dislocation density ρ_i and wall dislocation density ρ_w) to the flow stress are accounted for in a modified Taylor equation [61] as

$$\sigma = \sigma_0 + \alpha MGb\left(f_i\sqrt{\rho_i} + f_w\sqrt{\rho_w}\right), \tag{14}$$

where σ_0 is the basic yield strength, and α is the strengthening coefficient related to interior and wall dislocation densities.

From the above discourse, the set of constitutive equations is

$$
\begin{cases}
d\rho_i \Big/ dt = \dfrac{M\sqrt{\rho_i}}{Ab}\dot{\varepsilon} - 2BM\rho_i\dfrac{d_{crit}}{b}\dot{\varepsilon} - 2CD_d\dfrac{Gb^3}{k_BT}\left(\rho_i{}^2 - \rho_{eq}^2\right) - 2f_H\nu_H\rho_i\dfrac{1}{\delta_w} \\
\rho_w = f_s\dfrac{\theta_w}{2b}\pi\delta_w{}^2 \Big/ \left(\dfrac{4}{3}\pi\left(\dfrac{\delta_w}{2}\right)^3\right) \\
d\delta_w \Big/ dt = -f_r\dfrac{\sqrt{3}\dot{\varepsilon}b^{1/2}}{\theta_s{}^{3/2}\delta_s{}^2}\delta_w{}^{\nu_1} + f_c\nu_D b^2\sqrt{\rho_t}\left[\exp - \left(\dfrac{U_s - PV_a}{k_BT}\right)\right] \\
d\theta_w \Big/ dt = c_3\left(1 - \dfrac{\theta_w}{\theta_{sat}}\right)\dfrac{b\dot{\varepsilon}\delta_w}{2n}\dfrac{(1-\alpha_s)}{\alpha_s}\left(2BM\rho_i\dfrac{d_{crit}}{b}\dot{\varepsilon} - 2CD_d\dfrac{Gb^3}{k_BT}\left(\rho_i{}^2 - \rho_{eq}^2\right)\right)\gamma^{c_2}, \\
\sigma = \sigma_0 + \alpha MGb\left(f_i\sqrt{\rho_i} + f_w\sqrt{\rho_w}\right) \\
P = \dfrac{4\gamma}{\delta_w}, \text{ with } \gamma = \gamma_m\dfrac{\theta_w}{\theta_m}\left(1 - \ln\left(\dfrac{\theta_w}{\theta_m}\right)\right) \\
V_a = \dfrac{b^3}{\theta_w}
\end{cases}
\tag{15}
$$

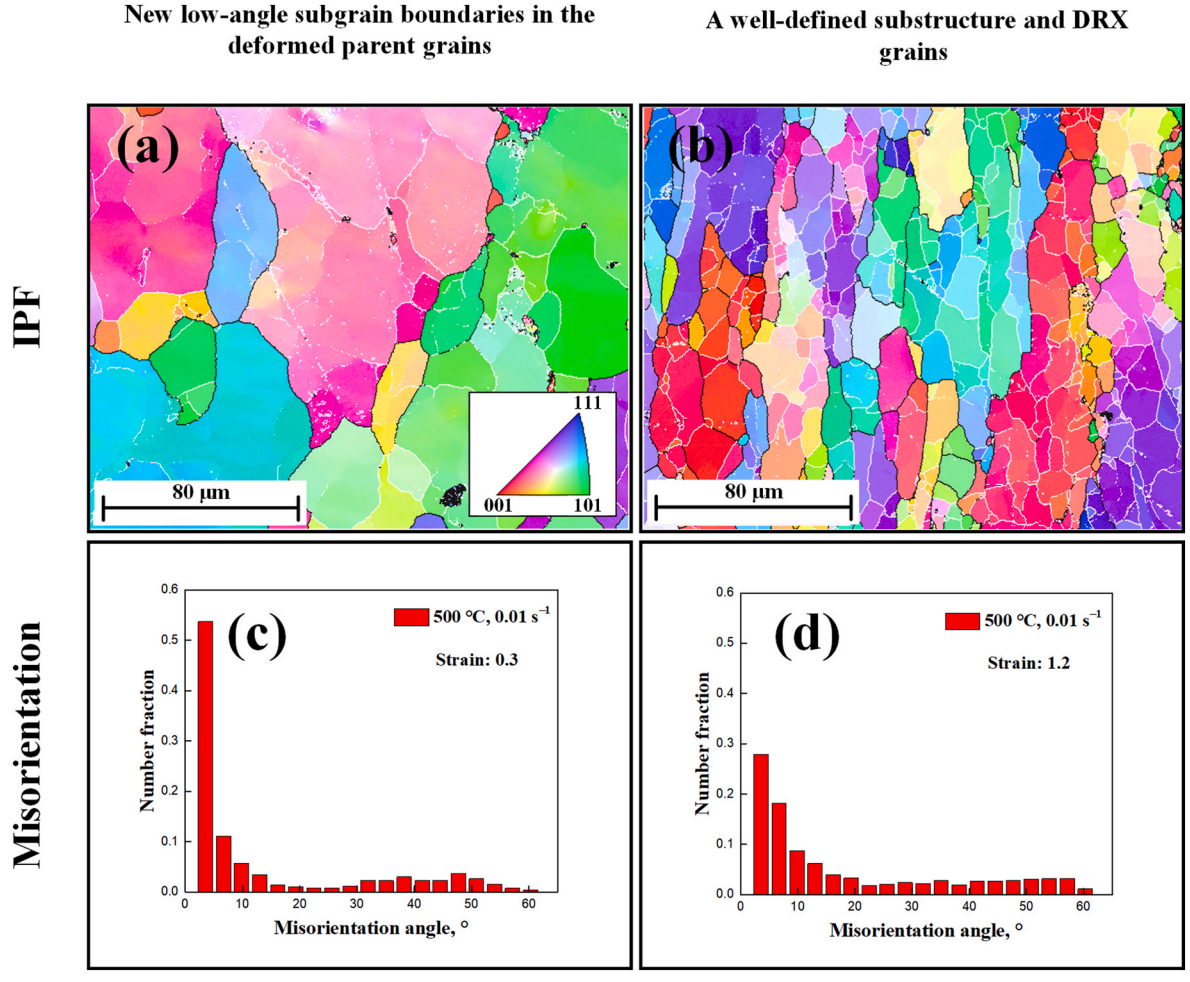

Fig. 3. EBSD images of AA1050 Al alloy deformed to a different strain at a temperature of 500 °C and a strain rate of 0.01 s^{-1}: (a)–(b) inverse pole figure (IPF) maps of the specimens deformed with strain 0.3 and 1.2, and (c)–(d) corresponding distribution histograms of misorientation angle.

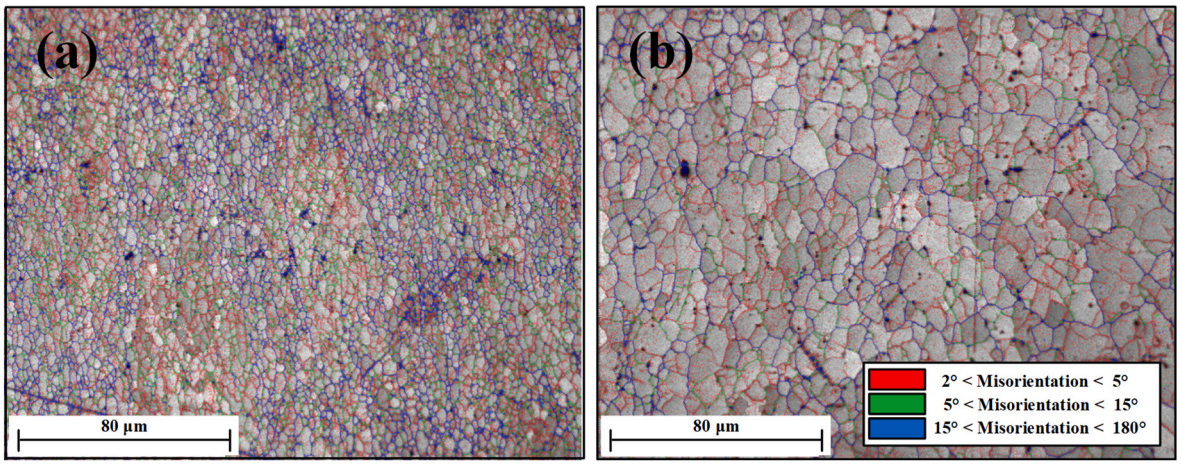

Fig. 4. Grain boundary maps of the specimens deformed to strain 0.9 under different deformation condions of (a) 400 °C/0.1 s^{-1}, and (b) 500 °C/0.1 s^{-1}.

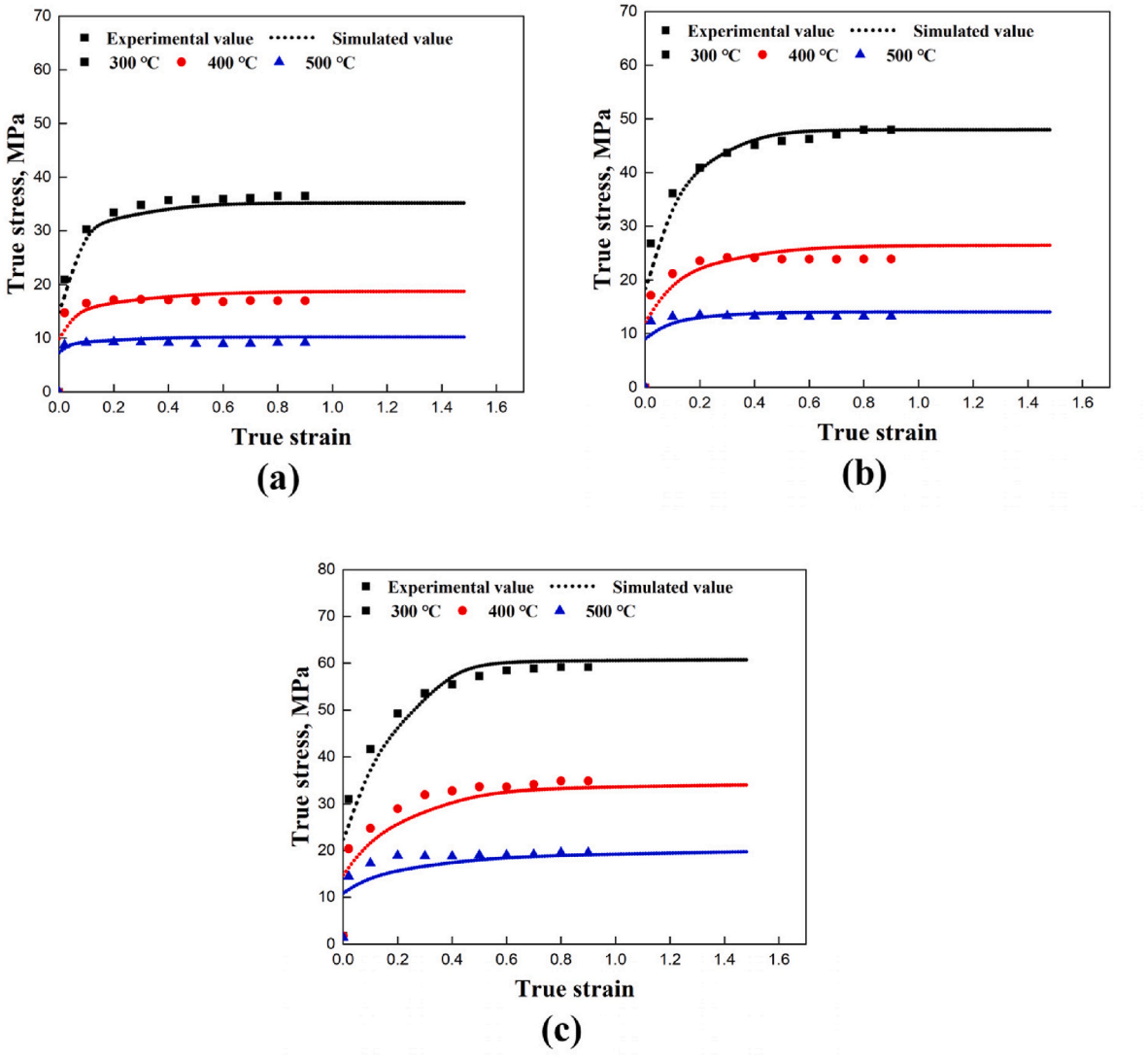

Fig. 5. The comparison between the experimental and simulated values of the flow stress with different deformation conditions of (a) 0.01 s^{-1}, (b) 0.1 s^{-1}, and (c) 0.8 s^{-1}.

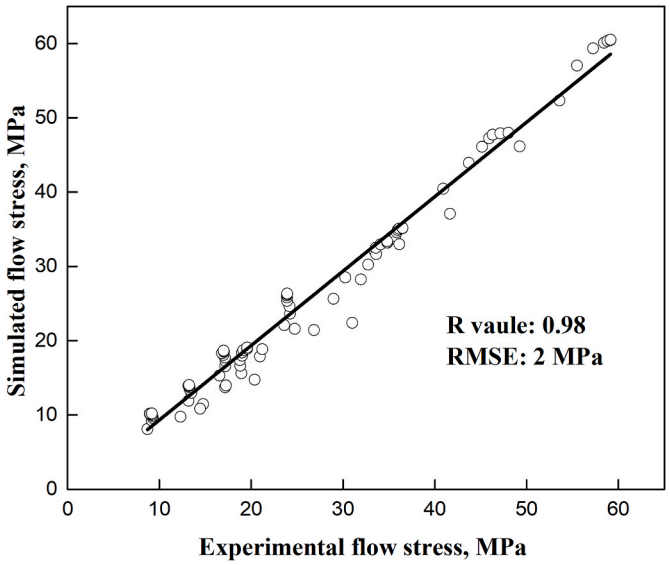

Fig. 6. Error analysis for the dislocation-based model.

The integration of the rate equations is performed with the MATLAB software version R2016b. The simulation results and discussion are presented in the following section.

4. Results and discussion

4.1. Model input parameters for AA1050 Al alloy

The initial average subgrain size δ_0 is set to 100 μm, and the initial subgrain boundary misorientation is assigned a non-zero value of 0.05°. The value of the activation energy Q is 142 kJ mol^{-1} for pure Al [62]. The energy of HAGBs γ_m is taken as 0.324 J m^{-2}, as suggested by Murr [63]. The activation energy for self-diffusion in Al [64] is $2{\cdot}10^{-19}$ J. atom^{-1}. The input parameters of the subgrain size evolution model have been reported in a previous paper [46]. The dislocation density evolution parameters can be found in the literature as suggested by Sherstnev, Lang, and Kozeschnik [23], Kreyca and Kozeschnik [52], and Gourdet and Montheillet [39]. The initial interior dislocation density is set to $1{\cdot}10^{11}$ m^{-2} [23,52], and the initial wall dislocation density is calculated from the initial value of the microstructure variables in Eq. (7).

The fraction coefficient α_s is taken as 0.5 and the saturated misorientation angle with continuing deformation θ_{sat} is 5°. The material constants c_2 and c_3 are set to 0.75 and 50, respectively. The basic yield strength $\sigma_0 = 1.1[\dot{\varepsilon} \bullet \exp(Q/RT)]^{0.1}$. The strengthening coefficient α is taken as 0.2. The other input parameters for the model are summarized in Table 1.

4.2. Model application and discussion

4.2.1. Experimental

The material investigated in this research is an AA1050 aluminum alloy provided by Neuman Aluminium Austria GmbH (Marktl, Austria). Single-pass isothermal compression experiments are conducted at temperatures of 300 °C, 400 °C and 500 °C, strain rates of 0.01 s^{-1}, 0.1 s^{-1} and 0.8 s^{-1}, and true strain 0.3, 0.6, 0.9, and 1.2, using a deformation dilatometer DIL 805 A/D (Hüllhorst, Germany). Previous studies [20, 46] have indicated the history of compression experiments. The true strain values are determined within the deformation dilatometer: true strain $= \mathrm{Ln}(L/L_0)$, where L_0 and L represents the initial length of the sample and the length after deformation, respectively.

The corresponding experimental results are presented in Fig. 3. The detailed parameters of the electron backscatter diffraction (EBSD) experiment are reported in a previous publication [20], . A duplex subgrain/grain structure is observed, with the recovered microstructure showing numerous low-angle subgrains within the elongated parent grains due to DRV. Additionally, some recrystallized grains have formed as a result of DRX. These features are characteristics of a dominant CDRX mechanism [9–12].

The refinement of subgrains plays a crucial role, with the average subgrain size being highly sensitive to the deformation parameters [46–50]. The average size of the newly CDRX recrystallized grains is nearly identical to that of the subgrains, further supporting the transformation of low-angle subgrain boundaries into HAGBs, and in agreement with results from Huang and Logé [10]. As plastic strain increases, the gradual accumulation of dislocations along subgrain boundaries accelerates the formation of HAGBs, thereby increasing the average misorientation angle. Fig. 3c and (d) shows the corresponding distribution of misorientation angles under various strains. The low-angle subgrain boundaries represent the major fraction for both strain conditions, accounting for 75% and 65%, respectively. This observation indicates that subgrain boundaries continue to form extensively even at high strain. Additionally, a gradual increase in subgrain boundary misorientation is observed with increasing strain.

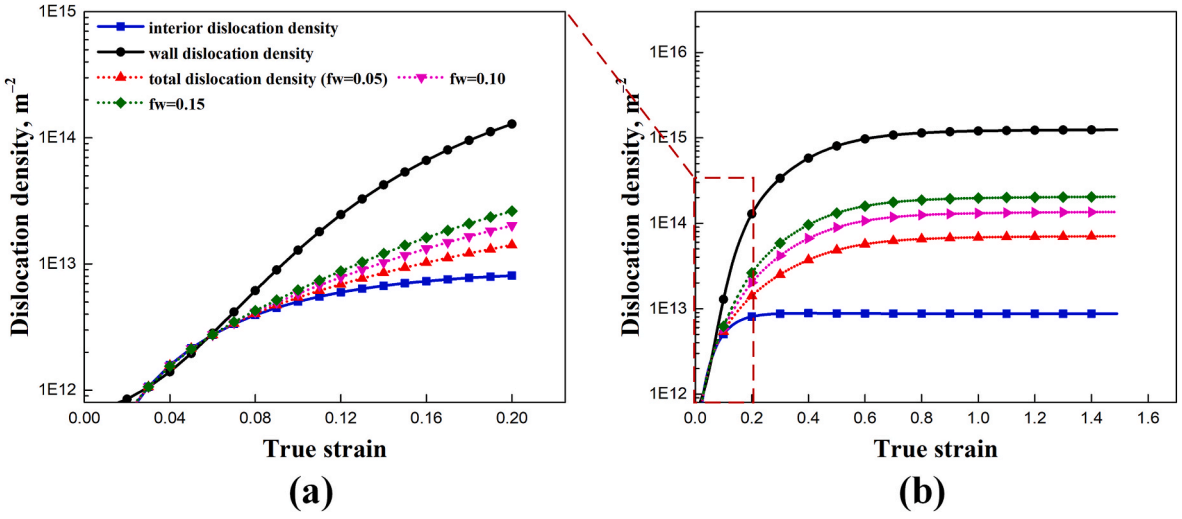

Fig. 7. Simulated total dislocation density (ρ_t), dislocation densities in the cell walls (ρ_w), and cell interiors (ρ_i) at 400 °C/0.1 s^{-1} of (a) strain 0.2 (the initial stage), and (b) strain 1.5.

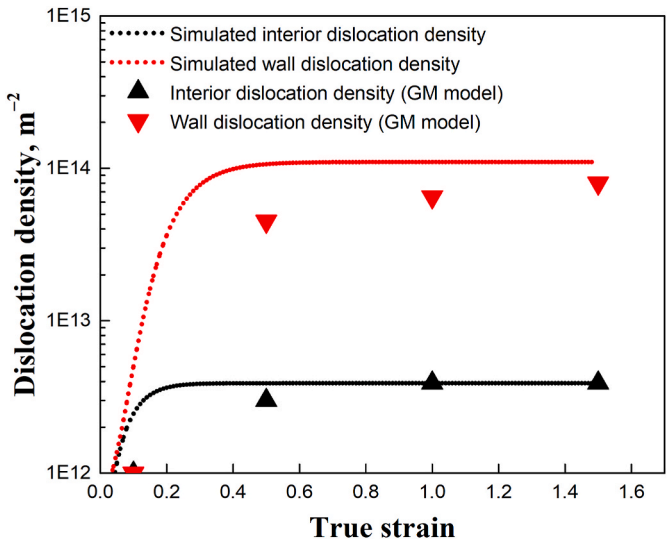

Fig. 8. Comparing the simulated dislocation density with the results from Gourdet and Montheillet [39].

Fig. 4 shows the grain boundary maps of the investigated alloy deformed at temperatures ranging from 400 to 500 °C and a strain rate of 0.1 s^{-1}. A significant number of low-angle subgrain boundaries (2° < misorientation angle <15°) are formed at a medium temperature of 400 °C due to dislocation accumulation. As the temperature increases, the gradually enlarging subgrains can be observed with enhanced boundary mobility [9–12]. This illustrates the effect of temperature on the substructure evolution and subgrain/recrystallized size. According to the research in literature [9–12,20,46], strain rate will also affect the microstructure variables during deformation. These variable effects will be incorporated into the dislocation-based model.

4.2.2. Flow curves

The flow curves obtained from the experiments are represented by symbols in Fig. 5. Subsequent simulations are performed using MATLAB software with one single set of input parameters (refer to Section 4.1) for all deformation conditions.

At the onset of deformation, work hardening (WH) dominates, caused by the multiplication and tangling of dislocations, which results in a continuous increase in flow stress. Simultaneously, numerous new subgrain boundaries are formed during compression, resulting in a rapid reduction of the average subgrain size [9,10]. As deformation commences, the dynamic softening mechanisms become increasingly prominent and eventually balance the continuous generation of dislocations [39–43]. The analysis indicates that the dislocation-based model potentially reproduces the measured flow curves.

To further evaluate the performance of the dislocation-based model, the correlation coefficient (R) and root mean square error ($RMSE$) [71] are evaluated as

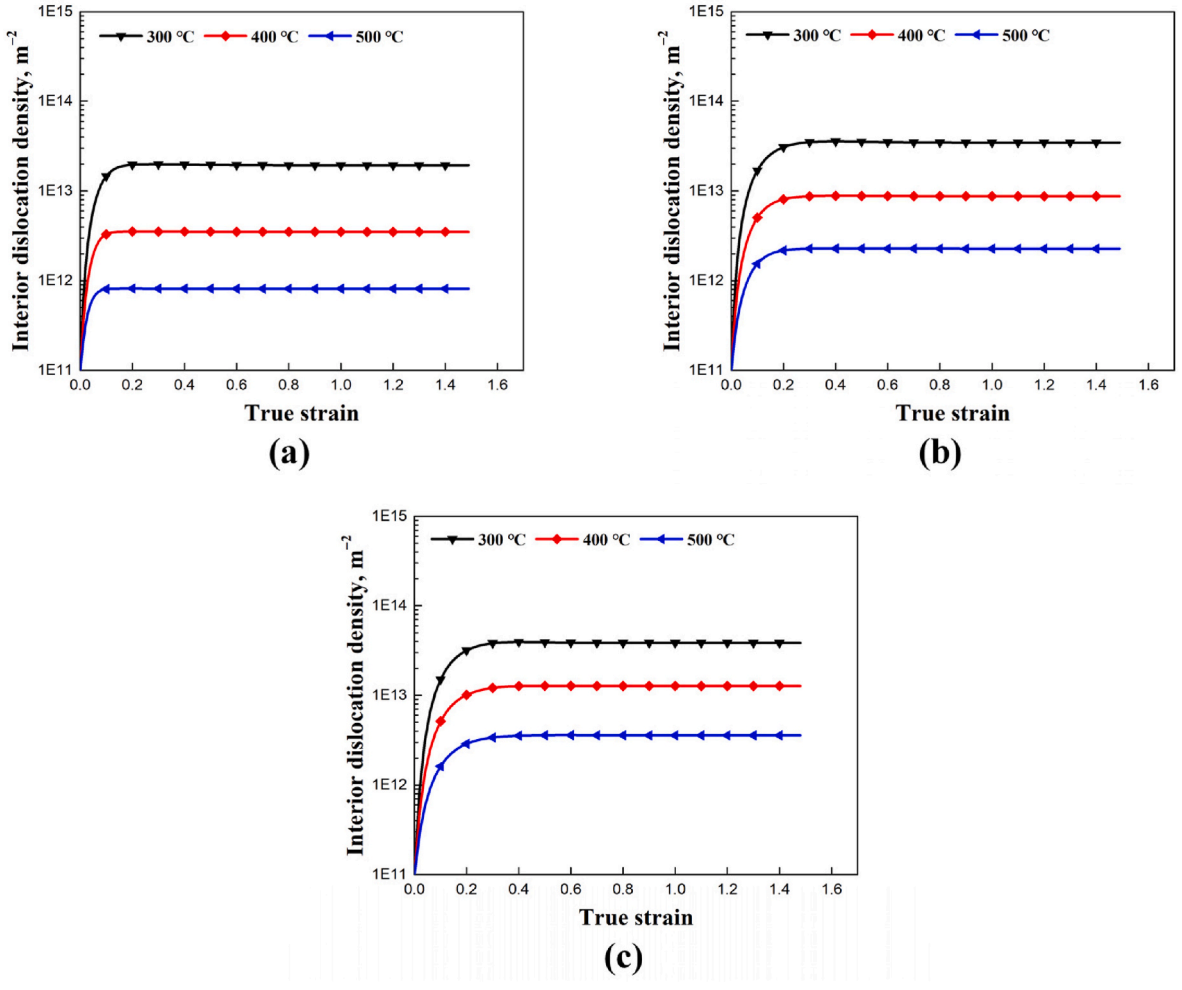

Fig. 9. Simulated interior dislocation density (ρ_i) at different deformation conditions: (a) 0.01 s^{-1}, (b) 0.1 s^{-1}, and (c) 0.8 s^{-1}.

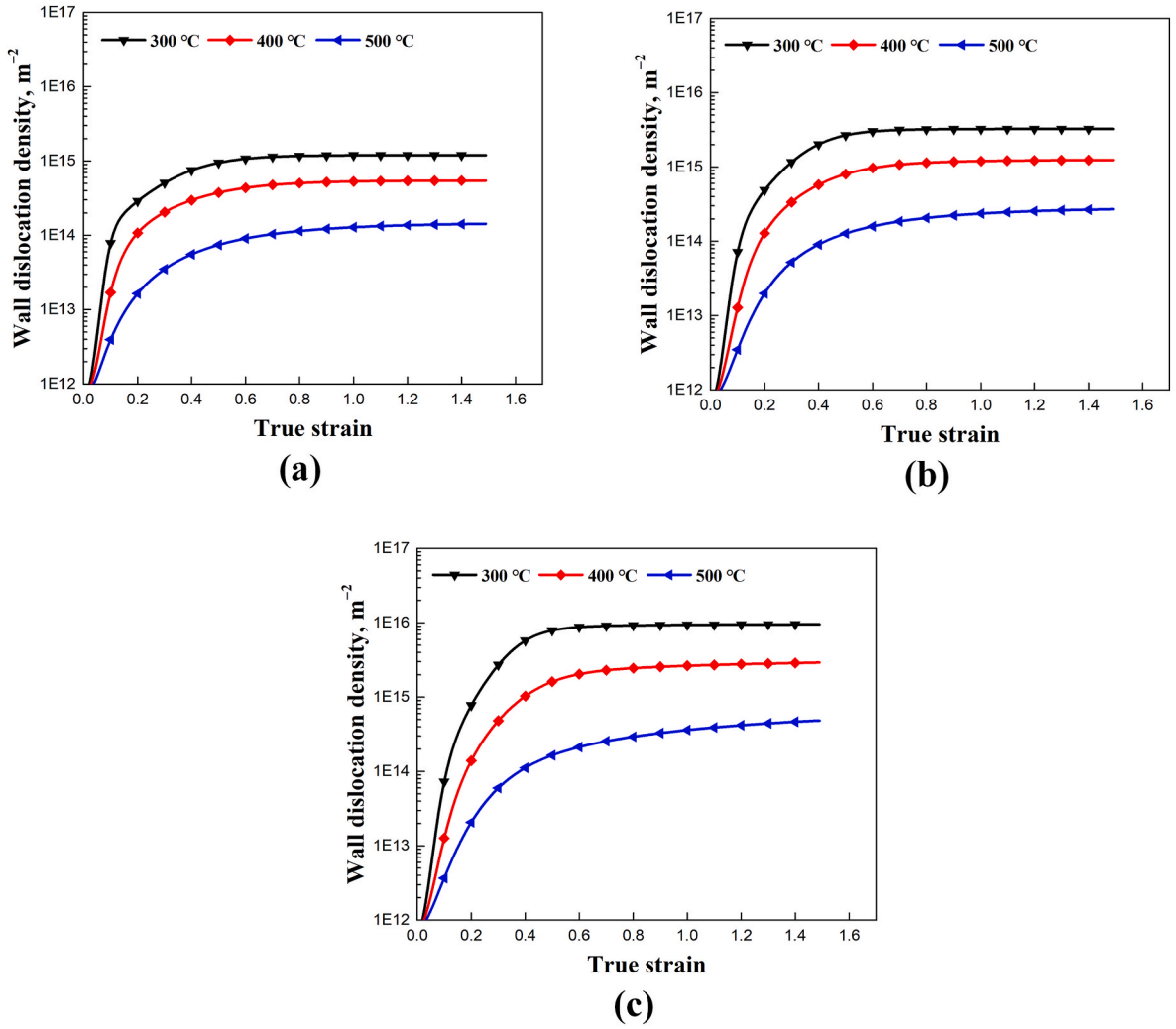

Fig. 10. Simulated wall dislocation density (ρ_w) at different deformation conditions: (a) 0.01 s^{-1}, (b) 0.1 s^{-1}, and (c) 0.8 s^{-1}.

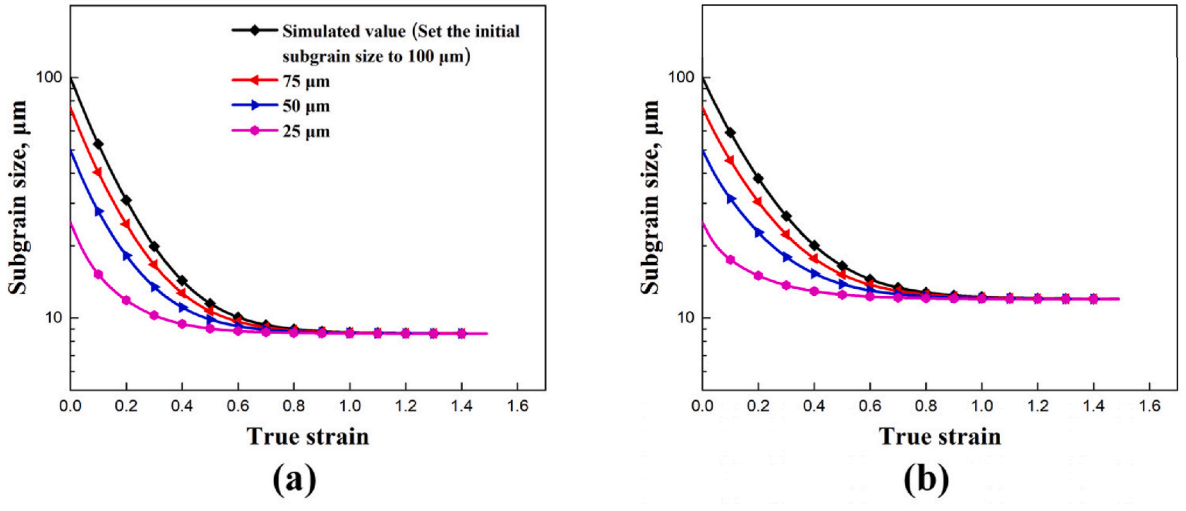

Fig. 11. (a). Evolution of simulated average subgrain size under various deformation temperatures and strain rates of (a) 350 °C/0.01 s^{-1}, and (b) 400 °C/0.01 s^{-1}.

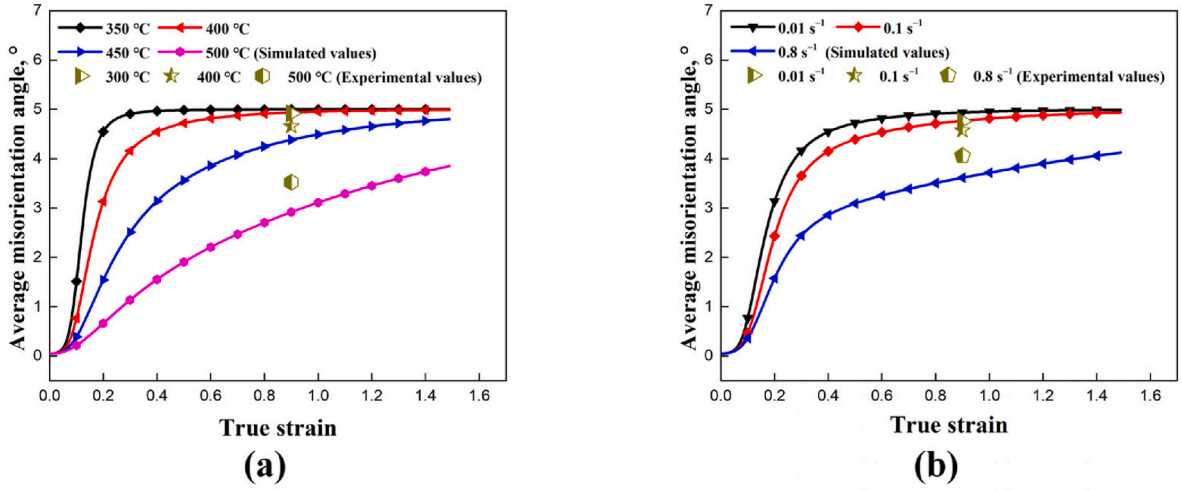

Fig. 12. Simulated average subgrain misorientation angle (θ_w) at different deformation conditions: (a) 0.01 s^{-1}, and (b) 400 °C.

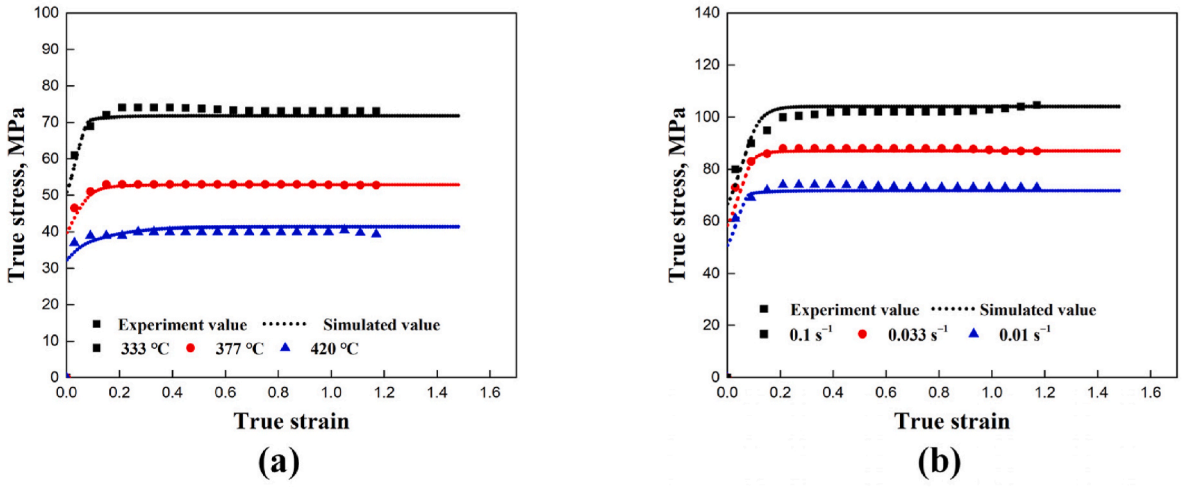

Fig. 13. The comparison between the experimental and simulated values of the flow stress with different deformation conditions of the AA5052 alloy: (a) 0.01 s^{-1}, and (b) 333 °C.

$$R = \frac{\sum_{i=1}^{N}(\delta_{ei} - \overline{\delta}_e)(\delta_{ci} - \overline{\delta}_c)}{\sqrt{\sum_{i=1}^{N}(\delta_{ei} - \overline{\delta}_e)^2 \sum_{i=1}^{N}(\delta_{ci} - \overline{\delta}_c)^2}}, \tag{16}$$

$$RMSE = \sqrt{\frac{1}{N}\sum_{i=1}^{N}(\delta_{ci} - \delta_{ei})^2} \cdot 100\%, \tag{17}$$

where δ_{ci} represents the calculated flow stress, δ_{ei} represents the experimental flow stress, $\overline{\delta}_c$ is the average calculated flow stress, $\overline{\delta}_e$ is the average experimental flow stress, and N is the total number of data points used in this study. The corresponding error analysis for different tested conditions is shown in Fig. 6. The values of R and $RMSE$ are 0.98 and 2.0 MPa, respectively.

4.2.3. Evolution of dislocation density

By numerically solving Eq. (2) and Eq. (7), the dislocation densities in both, cell walls and cell interiors, are obtained and the total dislocation density is calculated using Eq. (1). Fig. 7 illustrates the simulated total dislocation density, as well as the dislocation densities in cell walls and cell interiors, at the temperature of 400 °C and a strain rate of 0.1 s^{-1}. The simulation results presented in Fig. 7 indicate that the interior dislocation density increases rapidly during the initial stages of deformation. This trend is easily reasoned when considering the hardening and softening mechanisms. As deformation progresses, the interior dislocation density reaches a plateau, reflecting a balance between the generation and annihilation of interior dislocations, in agreement with the observations of Prasad et al. [72].

As illustrated in Fig. 7, the wall dislocation density also increases rapidly in the early stages. Wall dislocations are closely associated with subgrain formation and misorientation angles, which leads to a distinct

Table 2
List of different input parameters for AA5052 Al alloy.

Symbol	Name	Unit	Value	Ref.
A	A parameter	(−)	$0.005 \bullet \exp(0.015T)$	This work
B	B parameter	(−)	2	This work
C	C parameter	(−)	$1 \bullet 10^{-3}$	This work
f_i	Fraction of interior dislocations	(−)	0.9	This work
f_w	Fraction of wall dislocations	(−)	0.1	This work

plateau in their development at larger strains. During compression, the density of wall dislocations rises as subgrains continue to form, reflecting the transformation of mobile interior dislocations into wall dislocations. The simulation results are consistent with the established 3IVM model [22,73], wherein the density of wall dislocations is calculated based on the annihilation of dipole dislocations ρ_{dip}, as $d\rho_w/dt = (1/f_w)(d\rho_{dip}/dt)$.

The simulated total dislocation density using different coefficients for the cell wall fraction f_w (Eq. (1)), is displayed in Fig. 7 by the dash-dotted lines. The total dislocation densities increase when increasing f_w, which leads to an increase in flow stress in the end.

A comparison between the simulated dislocation density from the Gourdet and Montheillet (GM) model [39] and our dislocation model is presented in Fig. 8. Gourdet and Montheillet simulated the interior and wall dislocation density of 1200-grade aluminum at 460 °C and a strain rate of 0.1 s^{-1} using the GM model. Similarly, we employed identical temperature and strain rate conditions in our study. The minor differences observed between the GM model and our results are likely attributable to differences in alloy composition. The results exhibit reasonable qualitative agreement.

Figs. 9 and 10 present the simulated results for the interior and wall dislocation densities at other deformation conditions. The dislocation density increases with decreasing temperature or increasing strain rate. Low temperatures promote the accumulation of dislocations and reduce their annihilation rate, resulting in a higher dislocation density, in accordance with the conclusions of Yang et al. [20,46]. Furthermore, according to Taylor's strength equation, the dislocation density decreases as temperature increases. Similarly, high strain rates promote the formation and rotation of low-angle subgrains and dislocation cells, which is consistent with findings reported by Sakai et al. [9].

4.2.4. Evolution of average subgrain size and subgrain misorientation angle

Fig. 11 shows the simulated results for the average subgrain size evolution, accounting for both, refinement and thermal coarsening of subgrains. The subgrain size gradually decreases and nearly saturates at a constant value, which is consistent with findings in the literature [1,9,10,46,48]. Subgrain refinement caused by continuous new subgrain formation is accompanied by subgrain growth at high temperatures. The migration of subgrain boundaries leads to thermally induced coarsening of subgrains, achieving a dynamic balance at higher strains [9,10]. Based on Eqs. (8)–(10), the material coefficient v_1 governs the rate of subgrain refinement during the rapid reduction stage. Concurrently, subgrain coarsening is influenced by dislocation density, driving force, activation volume, etc, of the subgrain boundaries.

The classical Hall-Petch relationship [74], expressed as $\sigma_{sub} = k_{sub}\delta_{sub}^{-1/2}$, describes the influence of grain boundaries and subgrain boundaries on material strength. Here, σ_{sub} is the low-angle subgrain size, and k_{sub} is a material constant for subgrain boundary strengthening. As illustrated in Figs. 2–4, EBSD experiments revealed the formation of a large number of new subgrain boundaries, which can enhance the material's strength and flow stress during deformation.

The simulated results in Fig. 12 show that the average subgrain misorientation increases continuously during deformation across all temperatures and strain rates. As suggested by McQueen and Kassner [60], the average misorientation angle in Al increases rapidly due to the formation of dislocation dipoles and the absorption of mobile dislocations. This increase continues until a critical misorientation angle is reached, which subsequently leads to the transformation of these boundaries into HAGBs. The evolution of subgrain misorientation can also be described by the classical relationship $\theta = b/L$, where L is the spacing between two neighboring dislocations [39–43]. The dislocation spacing is typically associated with the dislocation density in terms of $\rho^{-1/2}$ [39–43].

Our results for the deformed microstructure are in line with the measured evolution of average subgrain size and average misorientation angle of subgrain boundaries as dislocations accumulate [20,46]. A decrease in temperature promotes the generation of low-angle subgrain boundaries, resulting in a rapid increase in subgrain misorientation. For Al and Al alloys, the annihilation of dislocations and subgrain boundary migration are more likely to occur at elevated temperatures [10–12].

4.3. Model application to an AA5052 alloy

To verify the applicability of the proposed model across various Al alloys, the present model framework is tested against experimental results for the AA5052 Al alloy from Gourdet [75]. The experimental flow curves have been measured under different deformation conditions: Three temperatures at a strain rate of 0.01 s^{-1} and three strain rates at a temperature of 333 °C, as shown in Fig. 13. The comparison shows good agreement between the experimental and simulated flow stress values (Fig. 13). The input parameters for the constitutive model of the AA5052 alloy are provided below.

The dislocation density evolution parameters A, B, C, and other parameters are chosen to best fit the AA5052 alloy results. The parameters that differ from that of the AA1050 alloy are shown in Table 2, the others remain the same as the ones in Table 1. The value of the activation energy Q is 156 kJ mol^{-1} for the AA5052 alloy [76]. Due to the difference in flow stress, the value of the material coefficient c_1 is taken as 80, and the calculation of $\bar{\sigma}_s$ is temperature and strain rate-dependent, with $\bar{\sigma}_s = 1.20[\dot{\varepsilon}\bullet\exp(Q/RT)]^{0.15}$ MPa. The basic yield strength σ_0 is described as $\sigma_0 = 2.1[\dot{\varepsilon}\bullet\exp(Q/RT)]^{0.12}$.

5. Conclusions

A dislocation-based model framework for the deformation of Al alloys based on micro/substructure evolution is proposed. The model is designed to simulate the microstructural changes occurring during high-temperature compression, including the evolution of dislocation density, subgrain size, misorientation angles, and flow stress. The key findings of this study are:

(1) The main microstructural evolution mechanisms observed in Al alloys are investgated in present work, including dislocation densities, low-angle subgrain size, subgrain boundary misorientation, and flow stress. The accumulation of mobile dislocations into low-angle subgrain boundaries forms a substructure through DRV. Concurrently, interior dislocations annihilate during processes such as DRV, SRV, or CDRX. EBSD experiments are conducted to support the microstructure analysis. The formation of new subgrain boundaries leads to a rapid reduction in the average subgrain size as the misorientation angle increases. The results describe the dependence of the microstructural variables on deformation conditions such as temperature, strain rate, and strain.

(2) A physically based dislocation model is proposed with separate populations of interior and wall dislocation densities, which considers the individual kinetics of wall densities. The model demonstrates that the increase in wall dislocation density is positively correlated with the progressive formation of subgrain boundaries during deformation. This process is accompanied by average subgrain size and misorientation at the subgrain boundaries. Special substructure models are developed and combined for the subgrain size, misorientation angle, and macroscopic mechanical response. These models are based on physically founded parameters and are self-sustaining, eliminating the need for commonly used power-law formulations.

(3) The dislocation-based model framework is successfully applied and validated for AA1050 and AA5052 aluminum alloys. The model consistently predicts flow curves and substructure evolution.

Author Contributions

Conceptualization, Q.Y. and E.K.; Methodology, Q.Y., T.W., and E.K.; Validation, Q.Y. and E.K.; Formal analysis, Q.Y.; Investigation, Q.Y. and T.W.; Resources, E.K. and T.W.; Data curation, Q.Y. and T.W.; Writing – original draft, Q.Y. and E.K.; Writing – review & editing, E.K.; Visualization, Q.Y., T.W., and E.K.; Supervision, E.K.; Project administration, E.K.; Funding acquisition, Q.Y. and E.K. All authors have read and agreed to the published version of the manuscript.

Data availability statement

The raw data supporting the conclusions of this article will be made available by the authors on request.

Funding

Open access funding is provided by the library of TU Wien (TUW).

Declaration of competing interest

The authors declare that they have no known competing financial interests or personal relationships that could have appeared to influence the work reported in this paper.

Acknowledgements

Qi Yang appreciates the financial support from the State Scholarship Fund of China (No. 202107710006) during his PhD at TU Wien.

References

[1] Humphreys FJ, Hatherly M. Recrystallization and related annealing phenomena. second ed. Oxford: Elsevier; 2004.
[2] Doherty RD, Hughes DA, Humphreys FJ, Jonas JJ, Juul Jensen D, Kassner ME, McNelley TR, McQueen HJ, Rollet AD. Current issues in recrystallization: a review. Mater Sci Eng, A 1997;238:219–74.
[3] Yang YM, Li YF, Yi DW, Zhang QL, Fang XW, Wang Y, Chang TX, Chen YN, Gao YM, Huang K. Revealing the microstructure evolution mechanism and mechanical responses of a novel Al-Zn-Mg-Cu alloy by hot deformation process. J Mater Res Technol 2024;29:3699–710.
[4] Sakai T, Jonas JJ. Dynamic recrystallization: mechanical and microstructural considerations. Acta Metall 1984;32:189–209.
[5] Mirzadeh H. Grain refinement of magnesium alloys by dynamic recrystallization (DRX): a review. J Mater Res Technol 2023;25:7050–77.
[6] Wei DJ, Han LY, Lv ZF, Wang GC, Zhao GQ. Investigation of constitutive models and microstructure evolution during hot deformation and solution treatment of Al-Zn-Mg-Cu alloy. J Mater Res Technol 2024;32:1028–45.
[7] Liu W, Zhao YH, Zhang YT, Shuai C, Chen LW, Huang ZQ, Hou H. Deformation-induced dynamic precipitation of 14H-LPSO structure and its effect on dynamic recrystallization in hot-extruded Mg-Y-Zn alloys. Int J Plast 2023;164:103573.
[8] Harikrishna K, Bhowmik A, Davidson MJ, Kumar R, Anqi AE, Rajhi AA, Alamri S, Kumar R. Evaluation of constitutive equations for modeling and characterization of microstructure during hot deformation of sintered Al-Zn-Mg alloy. J Mater Res Technol 2024;28:1523–37.
[9] Sakai T, Belyakov A, Kaibyshev R, Miura H, Jonas JJ. Dynamic and post-dynamic recrystallization under hot, cold and severe plastic deformation conditions. Prog Mater Sci 2014;60:130–207.
[10] Huang K, Logé RE. A review of dynamic recrystallization phenomena in metallic materials. Mater Des 2016;111:548–74.
[11] Raabe D. 23 - recovery and recrystallization: phenomena, physics, models, simulation. In: Laughlin DE, Hono K, editors. Physical metallurgy. Oxford: Elsevier; 2014. p. 2291–397.
[12] Sakai T, Miura H, Goloborodko A, Sitdikov O. Continuous dynamic recrystallization during the transient severe deformation of aluminum alloy 7475. Acta Mater 2009;57:153–62.
[13] Jiang S, Lv JX, Shi ZS, Lin JG. A study of dynamic recovery and recrystallisation mechanisms in aluminium alloy AA7050 at different thermomechanical processing conditions. Mater Sci Eng, A 2024;914:147117.
[14] Long MJ, Jiang F, Su YM, Xiao ZY. Dynamic recrystallization mechanisms and microstructure evolution of a novel Al-Zn-Mg-Cu-Zr alloy by isothermal compression. J Mater Res Technol 2024;33:1740–55.
[15] Cheng ZN, Zhang CS, Chu GN, Liu ZY, Wang KZ, Meng ZJ, Chen L, Sun L, Zhao GQ. Dynamic precipitation and recrystallization behavior during hot deformation of Al-Zn-Mg-Cu alloy: experiment and modeling. Int J Plast 2024;178:103995.
[16] Liu Z, Liu WB, Luo W, Du PN, Wang XM, Pei JY, Zhang RQ, Liu HQ. Discontinous and continuous dynamic recrystallization of Fe-12.5Cr-4Al-2Mo-0.03Nb-0.08Y alloy during hot deformation. J Mater Res Technol 2024;28:831–43.
[17] McQueen HJ, Knustad O, Ryum N, Solberg JK. Microstructural evolution in Al deformed to strains of 60 at 400°C. Scr Mater 1985;19:73–8.
[18] Zhang RQ, Zheng JH, Jiang J. Dynamic recrystallisation: a quantitative study on grain boundary characteristics and dependence on temperature and strain rate in an aluminium alloy. Acta Mater 2024;278:120266.
[19] Canelo-Yubero D, Kovács Z, Thierry Simonet Fotso JF, Tolnai D, Schell N, Groma I, Poletti C. In-situ characterization of continuous dynamic recrystallization during hot torsion of an Al-Si-Mg alloy. J Alloys Compd 2020;822:153282.
[20] Yang Q, Wojcik T, Kozeschnik E. Continuous dynamic recrystallization and deformation behavior of an AA1050 aluminum alloy during high-temperature compression. Metals 2024;14:889.
[21] Mecking H, Kocks UF. Kinetics of flow and strain-hardening. Acta Metall 1981;29:1865–75.
[22] Goerdeler M, Gottstein G. A microstructural work hardening model based on three internal state variables. Mater Sci Eng, A 2001;309:377–81.
[23] Sherstnev P, Lang P, Kozeschnik E. In: Eberhardsteiner J, et al., editors. Eur. Congr. Comput. Methods appl. Sci. Eng. (ECCOMAS 2012), 10.-14.9.2012,; 2012. p. 1–8. Vienna, Austria.
[24] B Ferraz FM, Buzolin RH, Ebenbauer S, Leitner T, Krumphals A, Poletti MC. A predictive mesoscale model for continuous dynamic recrystallization. Int J Plast 2024;179:104022.
[25] Kocks UF. A statistical theory of flow stress and work-hardening. Philos Mag 1966;13:541–66.
[26] Bergström Y. A dislocation model for the stress-strain behaviour of polycrystalline α-Fe with special emphasis on the variation of the densities of mobile and immobile dislocations. Mater Sci Eng 1970;5:193–200.
[27] Bergström Y, Roberts W. The dynamical strain ageing of α-iron: effects of strain rate and nitrogen content in the jerky-flow region. Acta Metall 1973;21:741–5.
[28] Mecking H, Estrin Y. The effect of vacancy generation on plastic deformation. Scripta Metall 1980;14:815–9.
[29] Kocks UF, Mecking H. Physics and phenomenology of strain hardening: the FCC case. Prog Mater Sci 2003;48:171–273.
[30] Roters F, Raabe D, Gottstein G. Work hardening in heterogeneous alloys-a microstructural approach based on three internal state variables. Acta Mater 2000;48:4181–9.
[31] Hughes DA, Hansen N. High angle boundaries formed by grain subdivision mechanisms. Acta Mater 1997;45:3871–86.
[32] Hughes DA, Hansen N. The microstructural origin of work hardening stages. Acta Mater 2018;48:374–83.
[33] Estrin Y, Tóth LS, Molinari A, Bréchet Y. A dislocation-based model for all hardening stages in large strain deformation. Acta Mater 1998;46:5509–22.
[34] Tóth LS, Molinari A, Estrin Y. Strain hardening at large strains as predicted by dislocation based polycrystal plasticity model. J Eng Mater Technol 2002;124:71–7.
[35] Toth LS, Rollett AD. A model of strain hardening for stage IV based on lattice curvature induced dislocations and grain fragmentation. J Mater Res Technol 2024;30:4795–9.
[36] McQueen HJ, Ryan ND. Constitutive analysis in hot working. Mater Sci Eng, A 2002;322:43–63.
[37] Lin YC, Chen XM. A critical review of experimental results and constitutive descriptions for metals and alloys in hot working. Mater Des 2011;32:1733–59.
[38] Jonas JJ, Quelennec X, Jiang L, Martin É. The Avrami kinetics of dynamic recrystallization. Acta Mater 2009;57:2748–56.
[39] Gourdet S, Montheillet F. A model of continuous dynamic recrystallization. Acta Mater 2003;51:2685–99.
[40] Sun ZC, Wu HL, Cao J, Yin ZK. Modeling of continuous dynamic recrystallization of Al-Zn-Cu-Mg alloy during hot deformation based on the internal-state-variable (ISV) method. Int J Plast 2018;106:73–87.
[41] Chen SF, Li DY, Zhang SH, Han HN, Lee HW, Lee MG. Modelling continuous dynamic recrystallization of aluminum alloys based on the polycrystal plasticity approach. Int J Plast 2020;131:102710.
[42] Buzolin RH, Lasnik M, Krumphals A, Poletti MC. A dislocation-based model for the microstructure evolution and the flow stress of a Ti5553 alloy. Int J Plast 2021;136:102862.
[43] Ferraz FMB, Buzolin RH, Ebenbauer S, Leitner T, Krumphals A, Poletti MC. A predictive mesoscale model for continuous dynamic recrystallization. Int J Plast 2024;179:104022.
[44] Liu RX, Zhang ZW, Zhou GW, Jia ZH, Li DY, Wu PD. A polycrystal plasticity-cellular automaton integrated modeling method for continuous dynamic recrystallization and its application to AA2196 alloy. Int J Plast 2024;182:104127.
[45] Wang J, Liang CZ, Ouyang B, Zhang Z, Chang XS, Qi YS, Chen G, Chen Q. Mesoscale modeling of continuous dynamic recrystallization in Ti-10V-2Fe-3Al alloy. Int J Mech Sci 2024;271:109303.
[46] Yang Q, Wojcik T, Kozeschnik E. Subgrain size modeling and substructure evolution in an AA1050 aluminum alloy during high-temperature compression. Materials 2024;17:4385.
[47] Poletti C, Rodriguez-Hortalá M, Hauser M, Sommitsch C. Microstructure development in hot deformed AA6082. Mater Sci Eng, A 2011;528:2423–30.
[48] Nes E. Modelling of work hardening and stress saturation in FCC metals. Prog Mater Sci 1998;41:129–93.
[49] Nes E, Vatne HE, Daaland O, Furu T, Ørsund R, Marthinsen K. Physical modelling of microstructural evolution during thermomechanical processing of aluminium alloys. Trondheim, Norway: SINTEF; 1994. Report STF24 S94003.

[50] Gourdet S, Montheillet F. An experimental study of the recrystallization mechanism during hot deformation of aluminium. Mater Sci Eng, A 2000;283:274–88.
[51] Belyakov A, Tsuzaki K, Miura H, Sakai T. Effect of initial microstructures on grain refinement in a stainless steel by large strain deformation. Acta Mater 2003;51:847–61.
[52] Kreyca J, Kozeschnik E. State parameter-based constitutive modelling of stress strain curves in Al-Mg solid solutions. Int J Plast 2018;103:67–80.
[53] Buken H, Kozeschnik E. Modeling static recrystallization in Al-Mg alloys. Metall Mater Trans A 2021;52:544–52.
[54] Brinckmann S, Sivanesapillai R, Hartmaier A. On the formation of vacancies by edge dislocation dipole annihilation in fatigued copper. Int J Fatig 2011;33:1369–75.
[55] Stechauner G, Kozeschnik E. Assessment of substitutional self-diffusion along short-circuit paths in Al, Fe and Ni. Calphad 2014;47:92–9.
[56] Dronhofer J Pešička A, Eggeler G. Free dislocations and boundary dislocations in tempered martensite ferritic steels. Mater Sci Eng, A 2004;387:176–80.
[57] Marthinsen K, Nes E. Modelling strain hardening and steady state deformation of Al-Mg alloys. Mater Sci Technol 2001;17:376–88.
[58] Huang Y, Humphreys FJ. Subgrain growth and low angle boundary mobility in aluminium crystals of orientation {110}⟨001. Acta Mater 2000;48:2017–30.
[59] Furu T, Orsund R, Nes E. Substructure evolution during different hot deformation processes of commercial non-heat treatable aluminium alloys. Mater Sci Eng, A 1996;214:122–32.
[60] McQueen HJ, Kassner ME. Comments on 'a model of continuous dynamic recrystallization' proposed for aluminum. Scr Mater 2004;51:461–5.
[61] Taylor GI. The mechanism of plastic deformation of crystals. Part I. Theoretical. Proc Roy Soc Lond A 1934;145:362–87.
[62] Sherby OD, Klundt RH, Miller AK. Flow stress, subgrain size, and subgrain stability at elevated temperature. Metall Trans A 1977;8:843–50.
[63] Murr LE. Interfacial phenomena in metals and alloys. Reading, MA: Addison-Wesley; 1975.
[64] Federighi T. A possible determination of the activation energy for self-diffusion in aluminium. Philos Mag 1959;4:502–10.
[65] Hirth JP, Lothe J. Theory of dislocations. Krieger Publishing Company; 1991.
[66] Galindo-Nava EI, Rivera-Díaz-del-Castillo PEJ. A thermostatistical theory of low and high temperature deformation in metals. Mater Sci Eng 2012;543:110–6.
[67] Mecking H, Nicklas B, Zarubova N. A universal temperature scale for plastic flow. Acta Mater 1986;34:527–35.
[68] Frost H, Ashby M. Deformation-mechanism maps. first ed. Oxford: Pergamon Press; 1982.
[69] Bergström Y. The plastic deformation of metals-a dislocation model and its applicability. Rev Powder Metall Phys Ceram 1983;2:79–265.
[70] Tzanetakis P, Hillairet J, Revel G. The formation energy of vacancies in aluminium and magnesium. Phys Status Solidi 1976;75:433–9.
[71] Mirzadeh H, Cabrera JM, Najafizadeh A. Modeling and prediction of hot deformation flow curves. Metall Mater Trans A 2012;43:108–23.
[72] Prasad GVSS, Goerdeler M, Gottstein G. Work hardening model based on multiple dislocation densities. Mater Sci Eng 2005;400:231–3.
[73] Goerdeler M, Gottstein G. A microstructural work hardening model based on three internal state variables. Mater Sci Eng, A 2001;309:377–81.
[74] Hansen N. Hall-Petch relation and boundary strengthening. Scr Mater 2004;51:801–6.
[75] Gourdet S. *Étude des mécanismes de recristallisation au cours de la déformation a chaud de l'aluminium*. Matériaux. Français: Ecole Nationale Supérieure des Mines de Saint-Etienne; 1997. Doctoral dissertation.
[76] Kowalski B, Lacey AJ, Sellars CM. Correction of plane strain compression data for the effects of inhomogeneous deformation. Mater Sci Technol 2003;19:1564–70.